Rene and Fokui
Journal of Engineering and Applied Science (2023) 70:97
https://doi.org/10.1186/s44147-023-00271-z

Journal of Engineering and Applied Science

RESEARCH Open Access

A quantum particle swarm optimization-based optimal LQR-PID controller for load frequency control of an isolated power system

Ebunle Akupan Rene[1*] and Willy Stephen Tounsi Fokui[2]

*Correspondence:
ebunleakupanrene@gmail.com

[1] Department of Electrical and Electronic Engineering, Catholic University of Central Africa (UCAC-ICAM), P.O Box 5504, Douala, Cameroon
[2] Teleconnect GmbH, Am Lehmberg 54, Dresden 01157, Germany

Abstract

One of the characteristics of a robust power grid is minimal variations in its frequency to load change or loss in generating unit(s). From the perspective of optimal control theory, the issue of load frequency control in the context of the interconnected functioning of power systems is investigated in this work, and a novel load frequency controller is proposed for a single area isolated power network. This novelty incorporates all the primary characteristics of the solutions that are based on a mixture of optimal controller designs by establishing a linear quadratic regulator optimized with quantum particle swarm optimization to design a proportional integral derivative (PID) controller unlike the conventional PID controller designs that are based on a combined Ziegler-Nichols and root locus (ZN-RL) method and manual tuning. The simulation results of the proposed controller using MATLAB show its efficacy in not only ensuring that there is no steady-state error in terms of the system frequency with load changes but also in achieving smoother transients. Following these landmark achievements, a transfer function model of the resulting power grid is constructed. The outcome of the model reveals that the system transients have been improved while keeping the intended steady-state characteristics. Furthermore, it is observed that the proposed load frequency controller has the best performance when compared with the combined ZN-RL method and the manual PID designs. This, therefore, demonstrates the superiority of the proposed design for load frequency control in power systems.

Keywords: Load frequency, Transfer function, Linear quadratic regulator, Particle swarm optimization, PID controller, Ziegler-Nichols

Introduction

The conventional power grid whose main purpose was to generate electricity in bulk at far away generating stations and transmitting it at high voltages to load centers through transmission lines is rapidly evolving with the introduction of distributed generation (DG), storage, and Internet of things [1]. All these have tremendously increased the complexity of the power grid and have brought in numerous challenges one of which being load frequency control (LFC) [2]. As the frequency of the network must always

be within set tolerances, frequency stability is a critical component of the power system. The tripping of big production units or tie lines, a sudden change in loads, or an imbalance between the power generated and the power requested by the loads are all examples of events that can cause frequency deviations [3]. Frequency response services are used by distribution service providers to balance the grid in real time by enabling generating units and loads to adjust their input or output powers in response to changes in the frequency of the power grid [4]. A lot of control strategies have been proposed in the literature for LFC of the power grid. The proportional-integral-derivative (PID) controller is of interest in this research work. PID controllers are one of the most prevalent controllers that are available for industrial applications because of their ease of use, straightforward functionality, and simplicity [5, 6]. PID controllers are used to accomplish both the improvement of the dynamic response and the reduction or elimination of the steady-state error.

Numerous scholars have proposed the use of PID controllers for the LFC of isolated power grids. In [7], the authors used active disturbance rejection control for the LFC of a power grid highly penetrated with wind power taking into consideration the randomness of the generated wind power. Simulation results demonstrated the effectiveness of their proposed solution over the conventional proportional integral (PI) controller and its ability in controlling the grid frequency within small margins. In [8], quadratic regulator approach with compensating pole technique is used to optimize the design of a PID controller to control the frequency of a single area as well as a multi-area power system. To demonstrate the robustness, the proposed design was tested with external disturbance, uncertainties in parameters, and nonlinearities such as governor dead band and generation rate constraint. The authors in [9] proposed a state feedback control based on proportional-integral observer (PI observer) to control the load frequency of an isolated single-area power grid. The result obtained was compared with those obtained with a state feedback control based on a full-state Luenberger observer, and the response of the former showed to be better than that of the latter. Two-degree-of-freedom (2DOF) controllers are proposed to control the frequency of a hybrid islanded power grid made up of a solar thermal power plant, a diesel generator, a wind turbine, fuel cells, and a battery bank in [10]. The results obtained were compared with the primitive PI controller, classical PID controller, and 2DOF-PI controllers. The researchers in [11] were able to control the load frequency of a multi-area power grid by using a fuzzy PID controller taking into account uncertainties in parameters in addition to external disturbances. The proposed design was observed to have good transient behavior, could reliably reject disturbances, and was not sensitive to changes in parameters. An optimum way of tuning the PID controller together with the corresponding transient droop compensator (TDC) for a hydraulic turbine is present in [12]. The suggested approach was based on the input guide vane servomotor's desired time response specification (DTRS), which covered typical rate limiters and gain saturation in power plants. In [13], the authors proposed a decentralized brain emotional learning-based intelligent controller (BELBIC) to control the frequency of a microgrid where in each DG is equipped with a BELBIC and particle swarm optimization (PSO) is used to get the parameters of the controller based on integral time square error (ITSE) criterion. The results obtained are compared

with those obtained using decentralized PID controllers, and also, fractional order PID (FOPID) controllers and their proposed design are shown to be outstanding. The research presented in [14] made used genetic algorithms, firefly, and bacterial foraging to tune decentralized PID controllers used for each generating unit/source in a microgrid. The simulation results demonstrated the superiority of firefly for the task compared to GA and BF.

This research aims at designing a linear quadratic regulator optimized with quantum particle swarm optimization proportional integral derivative (LQR-QPSO PID) controller for load frequency control of a single area power grid. The effectiveness of the proposed controller is validated by comparing its results with those obtained when the combined Ziegler-Nichols and root locus (ZN-RL) tuned, and manually tuned PID controllers are used. The contribution of this work to the body of knowledge is as follows:

- The utilization of QPSO to optimize the design of an LQR to tune a PID controller for load frequency control
- The design of the transfer function of the power grid with the proposed LFC integrate

The next section of this paper will elaborate on the methodology used in this research, followed by the presentation and discussion of the results and then a conclusion.

Methods

LFC strives to regulate the tie-line interchange schedules while also dividing the load between the generators of the same network, which is one of its operational goals. Other goals include maintaining a relatively constant frequency. The variation in frequency and the active power of the tie-line network are both detected, and this provides a measure of the variation in the rotor angle δ. This change in δ provides an error $\Delta\delta$ that has to be minimized. The corresponding change (error signal) in frequency Δf and real power of the tie line $\Delta P_{tie\ line}$ are amplified, combined, and converted into a real power command signal ΔP_{valve} before being sent to the prime mover (turbine). This signal command goes to request for an increase or a decrease in the torque being produced by the machine. To modify the values of Δf and $\Delta P_{tie\ line}$ within the required tolerance, the prime mover changes the generator output by an amount ΔP_{gen}. Figure 1 shows the block diagram of a power system with the load frequency control and automated voltage regulator.

Mathematical modeling of an isolated power system

The process of mathematically modeling a control system is the initial stage in its study and design. The state variable technique and the transfer function approach are the two most popular approaches. The state variable method may be used to represent both linear and nonlinear systems. The system must first be linearized before the linear state equations and transfer function can be used. In this work, the transfer function model has been created for the following elements using the right hypotheses and approximations to linearize the mathematical equations characterizing the system [15].

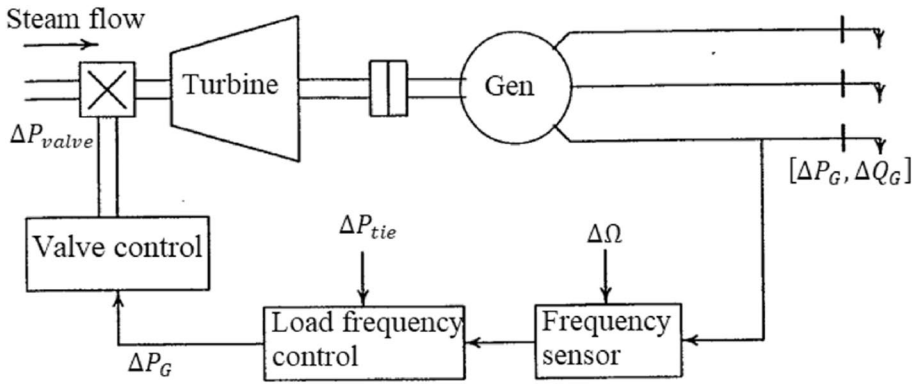

Fig. 1 Power system block diagram showing load frequency control and automated voltage regulator

Generator modeling

The power angle δ between the rotor axis and the resulting magnetic field is always kept constant while the machine is in its steady-state condition. Any disturbance will cause the rotor to slow down or speed up, causing a relative motion between the rotor and the air gap MMF (magneto-motive force). When there is no significant change in the total amount of power generated P_{elect}, the rotor will return to its starting position. The swing equation is the equation that accurately describes this relative motion as given by [1].

$$\frac{2H}{\omega_s}\frac{d^2\delta}{dt^2} = P_{mech} - P_{elec} \tag{1}$$

where P_{mech} and P_{elect} are respectively the per unit electrical and mechanical power, ω_s is the electrical angular velocity, and H is the per unit inertia constant defined by the following:

$$H = \frac{Total\ kinetic\ energy\ in\ MJ\ at\ rated\ speed}{machine\ rating\ in\ MVA} \tag{2}$$

H is measured in seconds and usually lies in the range $[1, 10]$ depending on the type or size of the machine.

For $\frac{d\delta}{dt}$ as a state variable, we obtain the following:

$$\frac{d\delta}{dt} = \Delta\omega \tag{3}$$

where $\Delta\omega$ is the angular frequency change of the grid due to perturbation. Hence, in terms of a small change in the angular velocity, Eq. (1) becomes as follows:

$$2H\frac{d\frac{\Delta\omega}{\omega_s}}{dt} = \Delta P_{mech} - \Delta P_{elect} \tag{4}$$

Expressing $\Delta\omega$ as per unit we obtain the following:

$$2H\frac{d\Delta\omega}{dt} = \Delta P_{mech} - \Delta P_{elect} \tag{5}$$

Transforming Eq. (5) as Laplace function yields the following:

$$\Delta\Omega(s) = \frac{\Delta P_{mech}(s) - \Delta P_{elect}(s)}{2Hs} \tag{6}$$

Load modeling

The load of a power system can be either resistive or reactive. However, only reactive loads like motors are sensitive to changes in the frequency of the power system. Their sensitivity depends on the combined speed-load characteristics of all the devices (loads) driven by the power system. The approximation of these characteristics can be represented by [16].

$$\Delta P_{elect} = \Delta P_{load} + D\Delta\omega \tag{7}$$

where ΔP_{load} denotes the change in the load that is not sensitive to frequency and $D\Delta\omega$ denotes the change in the load that is sensitive to frequency. The value of D is calculated by taking the percentage of change in load and dividing it by the percentage of change in frequency.

Taking the Laplace transform of Eq. (7) and combining it with Eq. (6) give the following:

$$\Delta\Omega(s) = \frac{\Delta P_{mech}(s) - \Delta P_{load}(s)}{2Hs + D} \tag{8}$$

$$\Delta\Omega(s) = \frac{K_{gen}}{\tau_{\text{gen}}s + 1}(\Delta P_{mech}(s) - \Delta P_{load}(s)) \tag{9}$$

where $K_{gen} = \frac{1}{D}$ is the power system gain and $\tau_{\text{gen}} = \frac{2H}{D}$ is the power system time constant.

Turbine modeling (prime mover)

The mechanical power provided by the prime mover may be derived from the mechanical action of hydraulic turbines at waterfalls or steam turbines whose energy is derived from the combustion of coal, gas, nuclear fuel, and gas turbines. The turbine model connects changes in mechanical power output ΔP_{mech} to changes in the steam valve position ΔP_{valve}. The simplest prime mover model (for a non-reheat steam turbine) may be approximated with a single time constant $\tau_{turbine}$, having the transfer function defined by Eq. (10). The time constant τ_{turbine} is usually between [0.2, 2] s [17].

$$G_{turbine}(s) = \frac{\Delta P_{mech}(s)}{\Delta P_{valve}(s)} = \frac{K_{turbine}}{\tau_{\text{turbine}}s + 1} \tag{10}$$

where $K_{turbine}$ is the gain factor of the turbine.

Governor modeling

The turbine governor detects the change in speed and adjusts the turbine input valve and mechanical power output to restore the speed to a constant state. Watt governors which are the earliest use rotating flyballs to detect speed and respond to variations in

speed with mechanical motion. The modem governors detect speed variations electronically. The governors are usually designed to allow the speed to decrease as the load demand increases to ensure stable operation. This variation between the speed and the load demand is governed by the speed regulation gain R.

Governors often have a 5 to 6% speed control from no load to full load. The governor speed mechanism functions as a comparator, with the output ΔP_{gov} equal to the difference between the reference power ΔP_{ref} and the power $\frac{1}{R}\Delta\omega$ as determined by the governor's speed characteristics [18]. That is as follows:

$$\Delta P_{gov} = \Delta P_{ref} - \frac{1}{R}\Delta\omega \tag{11}$$

Taking the Laplace transform of Eq. (9) gives the following:

$$\Delta P_{gov}(s) = \Delta P_{ref}(s) - \frac{1}{R}\Delta\Omega(s) \tag{12}$$

A large amount of force is usually needed to operate the steam/hydro turbine valves. This force comes from the hydraulic amplifier. It converts the command ΔP_{gov} to the steam valve position command ΔP_{valve}. With a linear connection and a time constant τ_{gov}, we get the relation in the Laplace domain as below.

$$\Delta P_{valve}(s) = \frac{K_{gov}}{\tau_{\text{gov}}s + 1}\Delta P_{gov}(s) \tag{13}$$

where K_{gov} is the speed governor gain.

Load frequency control of a single area network

In the process of modeling the power system for a single-area network, the development of the integrated structure of the speed governor, turbine, and generator load has to be formulated. Combining Eqs. (9), (10), (12), and (13) in a block diagram yields the complete schematic representation of a single area network as shown in Fig. 2.

Transfer function model

The steady-state analysis may be carried out by assuming that the speed changer is set to a fixed value, denoted by $\Delta P_{ref}(s) = 0$, while the demanded load changes. Free governor operation is the term used to describe this scenario.

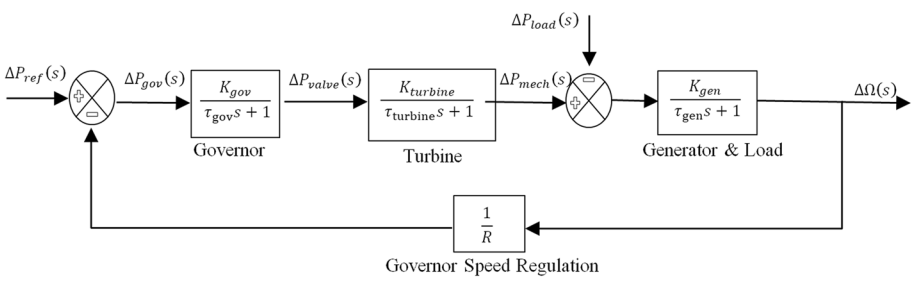

Fig. 2 Load frequency control of a single area isolated power system

Figure 3 is the result of redrawing the block diagram shown in Fig. 2 with the load change $\Delta P_{load}(s)$ serving as the input and the frequency deviation $\Delta\Omega(s)$ serving as the output. Equations (14) and (15) present respectively the open loop and the overall closed-loop transfer function of the design representing frequency change in response to load change.

$$G(s) = \frac{K_{gov}K_{turbine}K_{gen}}{R\left(\tau_{\text{gov}}\text{s}+1\right)\left(\tau_{\text{turbine}}\text{s}+1\right)\left(\tau_{\text{gen}}\text{s}+1\right)} \tag{14}$$

$$\frac{\Delta\Omega(s)}{-\Delta P_{load}(s)} = \frac{K_{gen}\left(\tau_{\text{gov}}s+1\right)\left(\tau_{\text{turbine}}s+1\right)}{\left(\tau_{\text{gov}}\text{s}+1\right)\left(\tau_{\text{turbine}}\text{s}+1\right)\left(\tau_{\text{gen}}\text{s}+1\right)+\frac{K_{gov}K_{turbine}K_{gen}}{R}} \tag{15}$$

K_{gov} and $K_{turbine}$ are respectively the static gains of the governor and turbine, and K_{gen} is the generator's gain which is the inverse of the damping coefficient D.

Steady-state analysis

For a unit step change in the load demand ΔP_D, the accompanying Laplace transform is given by the following:

$$\Delta P_{load}(s) = \frac{\Delta P_D}{s} \tag{16}$$

The frequency response now becomes the following:

$$\Delta\Omega(s) = \frac{-\Delta P_D K_{gen}\left(\tau_{\text{gov}}s+1\right)\left(\tau_{\text{turbine}}s+1\right)}{s\left[\left(\tau_{\text{gov}}\text{s}+1\right)\left(\tau_{\text{turbine}}\text{s}+1\right)\left(\tau_{\text{gen}}\text{s}+1\right)+\frac{K_{gov}K_{turbine}K_{gen}}{R}\right]} \tag{17}$$

Considering the final value theorem, the steady-state response of the frequency change can be obtained by the following:

$$\Delta\Omega_{e_{ss}} = \underset{s\to 0}{\text{Lim}} s\Omega(s) \tag{18}$$

$$\Delta\Omega_{e_{ss}} = \underset{s\to 0}{\text{Lim}} s\left\{\frac{-\Delta P_D K_{gen}\left(\tau_{\text{gov}}s+1\right)\left(\tau_{\text{turbine}}s+1\right)\left(\tau_{\text{gen}}s+1\right)}{s\left[\left(\tau_{\text{gov}}\text{s}+1\right)\left(\tau_{\text{turbine}}\text{s}+1\right)\left(\tau_{\text{gen}}\text{s}+1\right)+\frac{K_{gov}K_{turbine}K_{gen}}{R}\right]}\right\} \tag{19}$$

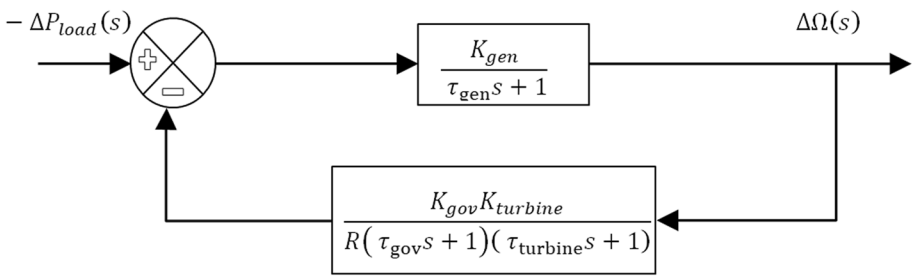

Fig. 3 Load frequency control of a single area network with load change as input and frequency change as output under free governor operation

$$\Delta\Omega_{e_{ss}} = \frac{-\Delta P_D K_{gen}}{1 + \frac{K_{gov}K_{turbine}K_{gen}}{R}} \tag{20}$$

Substituting for $K_{gen} = \frac{1}{D}$ gives the following expression for the steady-state value of the frequency.

$$\Delta\Omega_{e_{ss}} = \frac{-\Delta P_D}{D + \frac{K_{gov}K_{turbine}}{R}} \tag{21}$$

From Eq. (21), it can be seen that in the absence of a frequency-sensitive load (when $D = 0$), the steady-state deviation in frequency is determined by the governor speed regulation and the static gains of the turbine and the generator and is given by the following:

$$\Delta\Omega_{ss} = -\Delta P_D \frac{R}{K_{gov}K_{turbine}} \tag{22}$$

Load frequency control in response to load change

The purpose of the control strategy is to monitor and control the grid frequency with changes in load demand. The frequency response controller will need to be designed to robustly restore the frequency to its nominal value when a change in load occurs.

PID controller design

The proportional integral derivative (PID) controller is one of the most prevalent controllers that are available for purchase in commercial settings. The PID controller is used to accomplish both the improvement of the dynamic response and the reduction or elimination of the steady-state error. The derivative controller incorporates a finite zero into the open-loop plant transfer function, which helps to enhance the plant's reaction to transients. The integral controller raises the system type by one, adds a pole at the origin, and brings the steady-state error to zero. The time domain function used by the PID controller is as follows:

$$u(t) = K_p e(t) + K_i \int e(t)dt + K_d \frac{de(t)}{dt} \tag{23}$$

where K_p, K_i, and K_d are respectively the proportional, integral, and derivative gains of the controller, $u(t)$ is the control input, and $e(t)$ is the error signal. Equation (24) is Eq. (23) expressed in the s-domain.

$$U(s) = K_p + \frac{K_i}{s} + K_d s \tag{24}$$

The controller gains of the PID controller are calculated by picking the closed-loop poles that fulfill the performance criterion by appropriately optimizing the controller using swarm intelligence. This is done regardless of which controller is being used. PID controller design makes use of three distinct gains, which results in the introduction of two zeros and a pole at the origin of the system. This causes the system as a whole to become a type 1 system, which enables them to have no steady-state error.

The difficulty encountered during system controls using PID is locating the control rule vector $K = [K_p\, K_i\, K_d]$ of the controller, and as such, a more optimal control strategy is needed.

A change in system load will result in a steady-state frequency variance with the main LFC loop, dependent on the governor speed control. We must offer a reset operation to minimize the frequency deviation to zero. The rest action is accomplished by including an inbuilt proportional-integral-derivative controller that acts on the load reference setting to modify the speed set point. The proportional controller increases the speed of the response to bring the system to stability quickly. The integral controller raises the system type by one, causing the ultimate frequency deviation to equal zero. The derivative controller adds zero which helps enhance the system from heavy overshoots and oscillations. Figure 4 depicts the LFC system with the controller added. For an acceptable transient response, the controller gain $[K_p\, K_i\, K_d]$ must be adjusted.

From Fig. 4, the closed-loop transfer function is obtained assuming that the speed changer is set to a fixed value, denoted by $\Delta P_{ref}(s) = 0$, while the demanded load changes. This gives the following:

$$\frac{\Delta\Omega(s)}{-\Delta P_{load}(s)} = \frac{K_{gen}\left(\tau_{gov}s+1\right)\left(\tau_{turbine}s+1\right)}{\left(\tau_{gov}s+1\right)\left(\tau_{turbine}s+1\right)\left(\tau_{gen}s+1\right)+\frac{K_{gov}K_{turbine}K_{gen}}{R}\left(K_p+\frac{K_i}{s}+K_ds\right)} \tag{25}$$

Optimal PID design with combined Ziegler-Nichols tuning method and root locus

Ziegler and Nichols, who were Taylor Instruments employees, proposed two simple mathematical approaches for adjusting PID controllers in 1942. These approaches are now considered standard practice in the field of control systems. Both strategies involve a priori assumptions about the system model, but none requires these models to be explicitly understood. The first approach is used on plants that have step response; while the second method is used on plants that may be driven to instability with proportional control [2]. The Ziegler-Nichols formulas for controller specification are based on plant step responses. In this research, only the second method has been chosen because of its complex dynamics. The approach is intended to produce a closed-loop system with some acceptable percentage overshoot. However, this is most of the time not achieved since Ziegler and Nichols had predicted the changes on a unique plant model.

To move forward with the Ziegler-Nichols tuning procedure, it is needed to convert Eq. (23) into the form as follows:

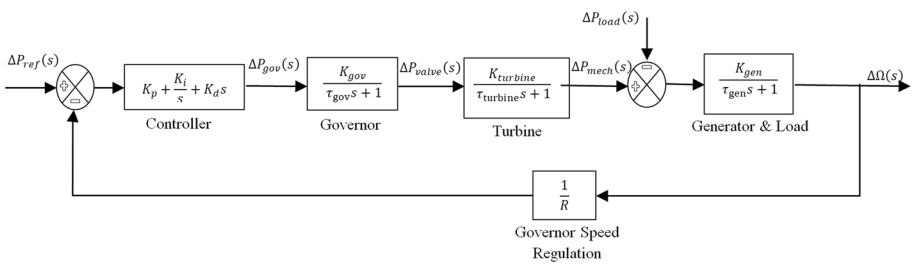

Fig. 4 LFC of an isolated power system

$$u(t) = K\left[e(t) + \frac{1}{T_i}\int e(t)dt + T_d\frac{de(t)}{dt}\right] \tag{26}$$

where,

$K_p = K$ is the proportional gain

$K_i = K_p/T_i$ is the integral gain

$K_d = K_p T_d$ is the derivative gain

T_i is the reset time (integration time constant)

T_d is the rate time (derivative time constant)

The tuning procedure is as follows:

- Step 1: The gain K is adjusted until the system bursts into continuous oscillations that neither decay nor explode.
- Step 2: The value of $K = K_c$ is noted for this condition. K_c is known as the critical or ultimate gain.
- Step 3: The oscillation is noted, and the period of the oscillation T_c is measured. T_c is known as the critical or the ultimate period.
- Step 4: K_p, T_i, and T_d are determined.
- Step 5: K_i and K_d are computed as a result.

According to the Ziegler-Nichols, the following Table 1 can be used to compute the $[K_p\, K_i\, K_d]$ gains. This research focuses on the design of a classical PID.

To start establishing the controller design using the Ziegler-Nichols method, the characteristic question $q(s)$ of the closed-loop system is obtained to compute the critical frequency since the response of the system is already known. $q(s)$ can be obtained following Eq. (25) with integral and derivative terms ignored and $K_p = K$.

$$q(s) = (\tau_{gov}s + 1)(\tau_{turbine}s + 1)(\tau_{gen}s + 1) + \frac{K_{gov}K_{turbine}K_{gen}}{R}K \tag{27}$$

The parameters used in this research for the generating power plant are shown in Table 2 [1].

The root locus diagram is obtained following the open-loop transfer function in Eq. (14) with a forward gain K (step 1 of the Ziegler-Nichols procedure). The governor speed regulation R is assumed to be constant.

Table 1 Ziegler-Nichols rule

Type of controller	$K_p = K$	T_i	T_d	$K_i = K_p/T_i$	$K_d = K_pT_d$
P-control	$0.5K_c$	∞	0	0	0
PI control	$0.45K_c$	$T_c/1.2$	0	$0.54K_c/T_c$	0
PD control	$0.8K_c$	∞	$T_c/8$	0	$0.1K_cT_c$
PID control (classical)	$0.6K_c$	$T_c/2$	$T_c/8$	$1.2K_c/T_c$	$0.075K_cT_c$
Pessen integration	$0.7K_c$	$2T_c/5$	$3T_c/20$	$1.75K_c/T_c$	$0.105K_cT_c$
Control with some overshoot	$K_c/3$	$T_c/2$	$T_c/3$	$(2/3)K_c/T_c$	$(1/9)K_cT_c$
Control with no overshoot	$0.2K_c$	$T_c/1.2$	$T_c/3$	$(2/5)K_c/T_c$	$(1/15)K_cT_c$

Table 2 Parameters used for LFC of an isolated power plant

Name	Parameter	Value
Governor gain	K_{gov}	1
The governor's time constant (s)	T_{gov}	0.2
Turbine gain	$K_{turbine}$	1
The turbine time constant (s)	$T_{turbine}$	0.5
Generator inertia time constant (s)	H	5
Percentage change in load divided by percentage change in frequency	D	0.8
Generator gain	$K_{gen} = 1/D$	1.25
The generator time constant (s)	$T_{gen} = 2H/D$	12.5
Governor speed regulation in p.u	R	0.05
Turbine-base MVA	P_{mech}	250
Nominal frequency (Hertz)	f	50
Change in load in p.u	ΔP_{load}	0.2

$$G(s) = \frac{K.K_{gov}.K_{turbine}K_{gen}}{R\left(\tau_{\mathrm{gov}}\mathrm{s}+1\right)\left(\tau_{\mathrm{turbine}}\mathrm{s}+1\right)\left(\tau_{\mathrm{gen}}\mathrm{s}+1\right)} \tag{28}$$

Substituting the parameters of the plant in Eq. (21) gives the following:

$$G(s) = \frac{25K}{(0.2\mathrm{s}+1)(0,5\mathrm{s}+1)(12.5\mathrm{s}+1)} \tag{29}$$

The basic goal of a root locus diagram is to predict the behavior of the closed-loop response using the root locus plot, which is derived from the open-loop transfer function. This plot shows the complex plane of the closed-loop pole locations. The root locus may be altered through the controller to provide the required closed-loop response by adding zeros and/or poles or simply shifting the closed-loop poles by adjusting K. K is given a value such that it drives the system to marginal instability under the given change in load demand. The root locus response is shown in Fig. 5.

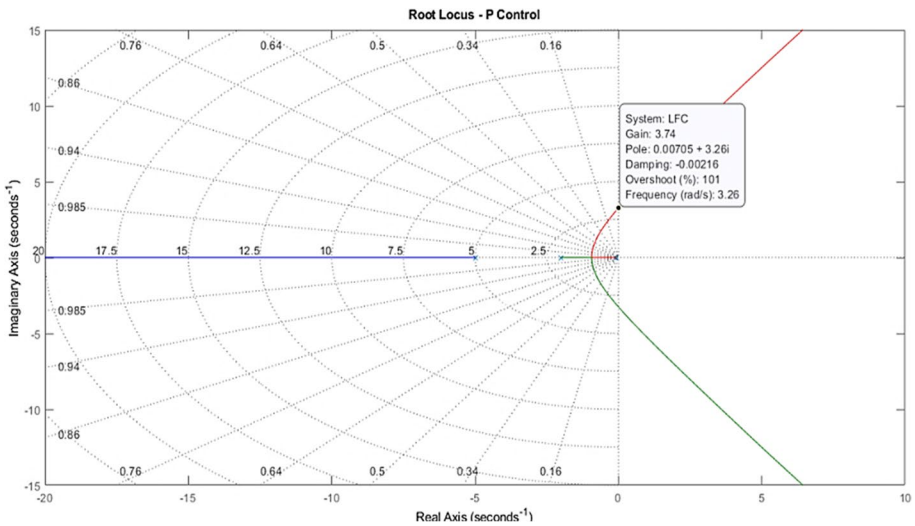

Fig. 5 Root locus plot for a gain $K = 1$

From the open-loop response of the root locus, the critical frequency ω_c is computed to deduce the gain at the point where the root locus crosses the stability boundary. This gain is K_c according to Ziegler Nichols since it is at this gain that the system will undergo an infinite simple harmonic motion.

$K_c = 3.74$ is the proportional gain at marginal stability. From the root locus plot, it can be seen that $s = \pm j3.26$ at the limit of stability. The control system is said to have a pair of conjugate poles on the $j\omega$-axis and is only marginally stable. Hence, marginal stability is obtained at around 14.96% of the overall system gain which is 25.

For $\omega = 3.26 rads/s$, a similar value of K_c is obtained using the system parameters and solving closed-loop characteristic equation $q(s) = 0$ in Eq. (27). The time response of the system at the critical gain is obtained and shown in Fig. 6 to compute the critical period T_c which is found to be 1.935 s. The above results are expressed in Table 3 below.

PID-based optimal LQR controller

The design of controllers in classical feedback control is based on output feedback. Such a control scheme is referred to as a feedback control scheme. The design of controllers in the state space is based on different feedback control scheme which is referred to as state feedback scheme. The use of state feedback gives the possibility of designing controllers with properties that cannot be obtained from classical feedback controllers. In this work, a state feedback controller known as a linear quadratic regulator (LQR) has been used to optimally design a PID controller for load frequency control. LQR is the

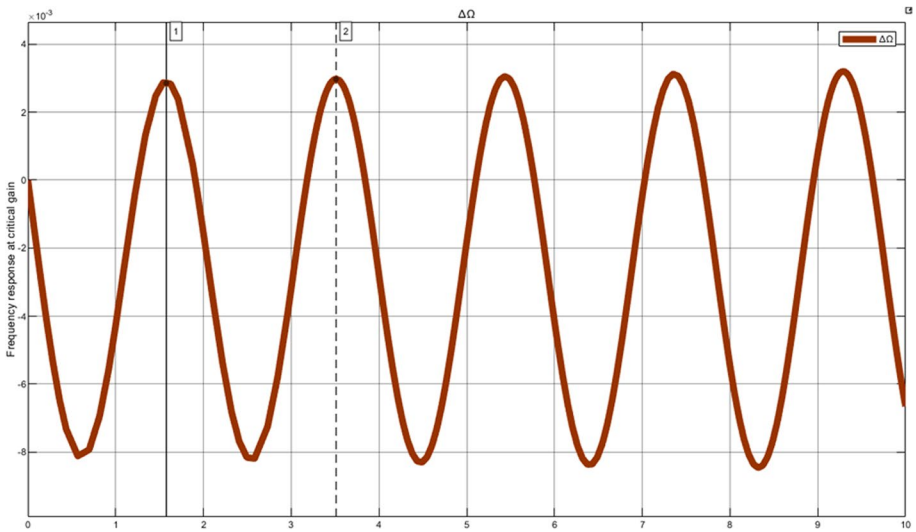

Fig. 6 Frequency response with change in load under critical gain

Table 3 Combined ZN-RL controller design parameters

Critical gain (K_c)	3.74
Critical period (T_c)	1.935*s*
Critical frequency (ω_c)	$\pm j3.26\ rads/s$

designed optimal controller for linear systems with quadratic performance index and is based on minimal error and energy criteria [3].

The LQR is a state feedback controller which is designed to maintain the state vector $\widetilde{x}$, to the origin of the state space. The state vector here is $\widetilde{x} = [\Delta P_{valve} \Delta P_{mech} \Delta\Omega]^T$. If disturbance as a result of load change should cause $\widetilde{x}$ to shift from its nominal value $\widetilde{x}_0 = \left[\Delta P_{valve} \Delta P_{mech} \Delta\Omega\right]_o^T$ in the state space, the controller will act to bring back $\widetilde{x}$ as closed to $\widetilde{x}_0$ as possible (the origin). Another method of optimal control like pole placement is a feasible option but finding the best place put the closed-loop poles have not been intuitive in higher-order systems or system with more actuators or states. The control law is designed to minimize the following parabolic objective function, J:

$$J = \int_{T_o}^{T_f} \left[\widetilde{x}^T Q \widetilde{x} + u^T R u\right] dt \tag{30}$$

$$\text{Subject to } \dot{\widetilde{x}} = A\widetilde{x}(t) + Bu(t)$$

where Q is the positive semi-defined matrix and R is the real symmetric matrix, A is the state matrix, and B is the input gain matrix. If the marked minors of all the elements of Q matrix are not negative, Q matrix is a positive semi-defined matrix. The selection of Q and R elements is determined according to the weighted relations of state variables and control inputs. With LQR, pole locations are not selected but rather an optimal gain matrix K_{opt} is determined by choosing closed-loop characteristics that are important for the control operation. This may include characteristics like how well the system performs and how much effort is needed to get that performance.

The objective of optimal regulator design is the determination of the optimal control rule $u^*(t) = K_{opt}\widetilde{x}(t)$ for the combined system to reject the step disturbance from a change in load demand ΔP_{load}, which implies converging the initial states to zero and minimizing the cost function defined by Eq. (30). In most research paper, the minimization of the above quadratic cost function has followed solving the Riccati equation [3] which is the solution to the Lagrange multiplier or Hamiltonian equation when the dynamics of the system is known to enable obtaining the gain K_{opt} that returns the best control input u defined by Eq. (31). The Hamiltonian is a mathematically advanced description of dynamic systems, a concept from the theory of classical mechanics. It is also regarded as a more sophisticated form of the Lagrangian dynamic equation.

$$K_{opt} = -R^{-1}B^T P \tag{31}$$

where B and R are respectively the input matrix and weighting matrix that is specified in Eq. (30) and P is a symmetric positive definite matrix that is created by solving the algebraic Riccati equation that is described in Eq. (25) [4] and is a rich version of the Lyapunov equation (which solves a globally asymptotically stable system at zero input cost).

$$A^T P + PA - PBR^{-1}B^T P = -Q \tag{32}$$

where A represents the state matrix and Q represents the symmetric positive semi-definite weighting matrix as specified in Eq. (32) and P is a symmetric positive definite matrix satisfying the equation. That is the solution to the Riccati equation. At times,

Eq. (32) or the Lagrange multiplier equation [1] with higher dimension (system with a large number of state variables and control loops) may become difficult and expensive to solve. As a result, finding the best control input u which minimizes the objective function J to give the optimal PID parameters for a given Q and R that give K_{opt} need to be known by the controls engineer. In this research work, using the LQR method, the gain parameters of the PID controller are optimally determined stochastically using the swarm intelligence technique known as quantum particle swarm optimization.

Quantum particle swarm optimization

Kennedy and Eberhart created the particle swarm optimization (PSO) method in 1995, drawing inspiration from the social behavior of fish and birds. This method is based on evolutionary swarm intelligence and is used to address numerous optimization tasks [19]. Due to its few adjustable parameters, quick convergence, simplicity, and ease of coding, as well as the fact that the initial solution does not significantly affect its convergence, PSO has been frequently utilized to address a range of engineering tasks [20].

In PSO, there are two main concepts: the local optimum p_{best} and the global optimum g_{best}. The global optimum is the optimum solution obtained by the entire swarm, while the local optimum is the optimum solution obtained by every particle that makes up the swarm. Given a swarm with particles P, every particle i, in the swarm at iteration t, has a position vector $X_i^t = (x_{i1}x_{i2}x_{i3}\ldots x_{in})^T$ and velocity vector $V_i^t = (v_{i1}v_{i2}v_{i3}\ldots v_{in})^T$. Equations (33) and (34) are used to update these vectors during every iteration via j dimension.

$$V_{ij}^{t+1} = wV_{ij}^t + c_1 r_1^t \left(p_{best_{ij}} - X_{ij}^t\right) + c_2 r_2^t \left(g_{best_{ij}} - X_{ij}^t\right) \tag{33}$$

$$X_{ij}^{t+1} = X_{ij}^t + V_{ij}^{t+1} \tag{34}$$

where:

$i = 1, 2, 3, \ldots, P$ and $j = 1, 2, 3, \ldots, n, c_1$ *and* c_2 are learning factors and r_1^t and r_2^t are random numbers between 0 and 1.

From Eq. (26), we can see that there are three contributions to the movement of the particle in an iteration. On the other hand, Eq. (27) updates the position of the particle. The parameter w is an initial weight constant, usually positive for classical PSO, and serves to balance the global search (known as exploration in the case of being set with higher values) as well as the local search (known as exploitation when being set with lower values) [19].

The risk of getting trapped in the local optimum solution is a difficulty for the primitive PSO, which prevents it from ever obtaining the global best solutions [21]. Because of this, many variants of PSO have been developed over the years [22]. The quantum PSO (QPSO) was introduced by J. Sun et al. in [23], after being inspired by the convergence of PSO, followed by a detailed analysis of the behavior of each particle making up the swarm. In [24], it is derived that the complexity of the behavior of social organisms is far greater to be able to be simplified by linear equations as is the case of the classical PSO. The QPSO particle movement rhythm is very different from the classical PSOs. The position and velocity of a particle cannot be determined simultaneously because,

according to the quantum world's unpredictability theory, they become observable at any location in the search space with a given probability. In the case of infinite searching iterations, the global convergence of QPSO ensures that the global optimal solution is calculated. Experimental findings on several benchmark functions have shown the superiority of QPSO over the classical PSO making QPSO very promising over PSO [25].

The different steps associated with QPSO are outlined below:

- *Step I*: Generation of the initial random population of the swarm within the D-dimension's space boundaries
- *Step II*: Estimation of the fitness value of each particle
- *Step III*: Comparison of the actual fitness of each particle with its personal best (p_{best}). Should in case the actual fitness is greater than p_{best}, then p_{best} is updated with the actual fitness value.
- *Step IV*: Calculate the average best position (av_{best}) of all the P particles present in the swarm using Eq. (35) shown below.

$$av_{best} = \frac{1}{P}\sum_{j}^{P} av_{bestj} \tag{35}$$

- *Step V*: From the entire swarm, determine the actual overall best fitness and its coordinate and compare it with the global best (g_{best}). If is greater than the global best (g_{best}), then it becomes the new g_{best}.
- *Step VI*: Calculate the vector local focus of the particles.

$$VLF_{jd}^{jt} = rand1_{jd}^{jt} \times \left(p_{best\,jd}\right) + \left(1 - rand1_{jd}^{jt}\right) \times g_{best}$$

- *Step VII*: The position x_{jd} of the d^{th} dimension of the j^{th} particle is updated using Eq. (36).

$$x_{jd}^{jt} = VLF_{jd}^{jt} + \left[(-1)^{ceil\left(0.5+rand2_{jd}^{jt}\right)}\right] * \beta * \left|avbest - x_{jd}^{jt-1}\right| * log_e\left(\frac{1}{rand3_{jd}^{jt}}\right) \tag{36}$$

If $x_{jd}^{jt} < x_{min}^{d}$

Then

$$x_{jd}^{jt} = x_{min}^{d} + 0.25 * rand4_{jd}^{jt} * \left(x_{max}^{d} - x_{min}^{d}\right) \tag{37}$$

If $x_{jd}^{jt} > x_{max}^{d}$

Then

$$x_{jd}^{jt} = x_{max}^{d} - 0.25 * rand5_{jd}^{jt} * \left(x_{max}^{d} - x_{min}^{d}\right) \tag{38}$$

where $rand1$, $rand2$, $rand3$, $rand4$, and $rand5$ are random numbers between 0 and 1 and jt is the present iteration.

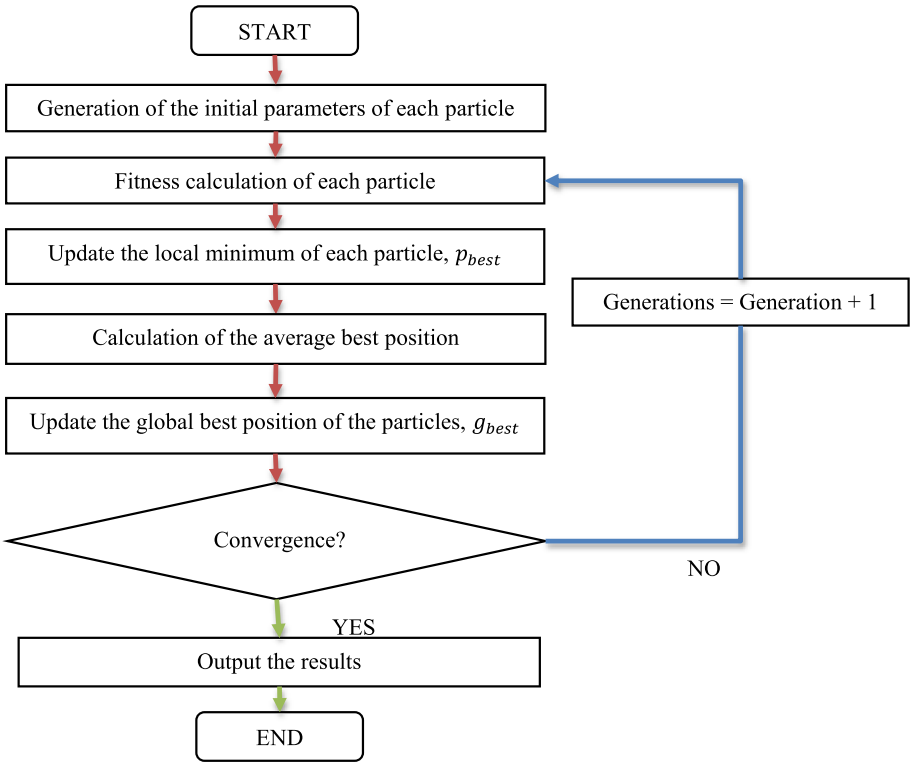

Fig. 7 Quantum particle swarm optimization algorithm flowchart [26]

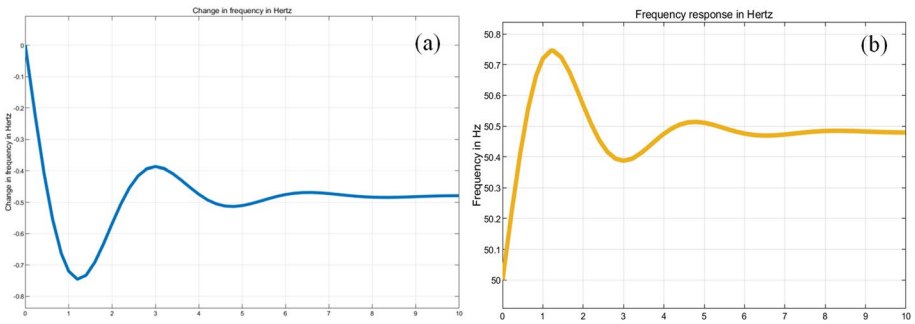

Fig. 8 No control: 0.2 p.u (50 MW) change in load. **a** Change in frequency in Hz. **b** Measured frequency in Hz

Equations (37) and (38) are applied in every dimension in the interval (x^d_{min}, x^d_{max}) to ensure that the particles do not exit the domain of interest.

The flowchart in Fig. 7 summarizes the operation of QPSO.

Results and discussion

System with no controller

According to the parameters provided in Table 2 as the plant parameters, when there is a step change in the load demand of 0.2 p.u. (50 MW), the following results shown in Fig. 8 are obtained. The frequency responses (the change in frequency and the measured frequency) related to a 0.2 p.u change in the load demand when the plant is under an uncontrolled state can be observed. The steady-state change in frequency Δf

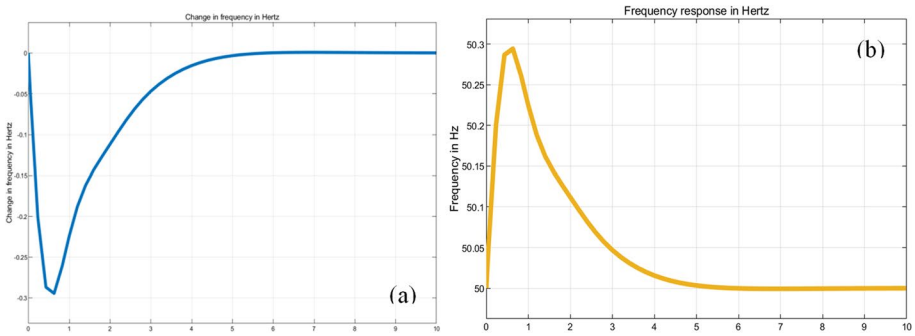

Fig. 9 PID control: manual tuning method: 0.2 p.u (50 MW) change in load. **a** Change in frequency in Hz. **b** Measured frequency in Hz

Table 4 PID (classical) control parameter from manual tuning

Parameter	Value
K_p	2.0121
K_i	0.9989
K_d	1.0117

is noticeable around 0.4794 Hz from the nominal system frequency, and it takes more than 6 s to transit to achieve this value. A maximum overshoot of 0.7437 Hz from the reference frequency also occurred. Though this may sound appealing in the context of control theory, however, for large changes in load, the frequency may run far from the normal and cause the system to be heavily unstable which has an adverse consequence on the generators as control action becomes very important.

System with manually tuned PID controller

When the control method that involves using PID that has been manually tuned is used as shown in Fig. 9, the change in frequency becomes more stable in comparison to the condition it was in before a controller was introduced. The time it takes to change the frequency in power networks must always not be too long (a requirement for every control) while also minimizing overshoots. This control system satisfies the requirements in certain respects with regard to stability. This system becomes acceptably stable before the 6-s mark before settling for a value of 1.267×10^{-4} Hz at 10 s unlike when a controller is not used. However, the system still suffers some degree of overshoot of 2.962×10^{-1} Hz which the controller could not remove. The controller design consideration was made to get the desired settling time while keeping the overshoot margin minimal. Using manual tuning to design a PID control may be one of the easiest ways towards designing this type of control, but this method becomes extremely challenging for complex systems with many control loop systems, and at times, finding the optimal gains can even be impossible. As a result, a classical design technique becomes handy as such a controller may not be very robust.

Table 4 below shows the result of the obtained PID gains from manual tuning.

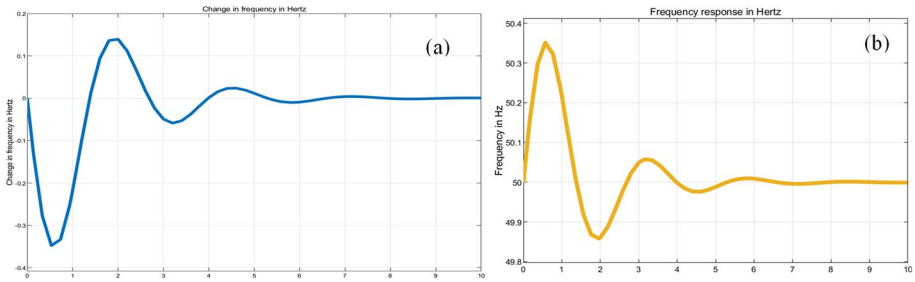

Fig. 10 PID control: combine Ziegler-Nichols and root locus method: 0.2 p.u (50 MW) change in load. **a** Change in frequency in Hz. **b** Measured frequency in Hz

Table 5 PID (classical) control parameter from combined Ziegler-Nichols and root locus

Parameter	Value: $K_c = 3.74$ *and* $T_c = 1.935$**s**	
K_p	$0.6K_c$	2.244
K_i	$1.2K_c/T_c$	2.31937984
K_d	$0.075K_cT_c$	0.5427675

Combine Ziegler-Nichols and root locus PID controller

The performance of the closed-loop step response using the combined Ziegler-Nichols and root locus method reveals a maximum overshoot difference of 3.485×10^{-1} Hz above the goal compared to the manual tuning which is less than 0.3 Hz. This is shown in Fig. 10.

The controller was still able to bring the power system frequency to acceptable stability after 8 s which was too long. The controller finally had a steady-state error of 7.038×10^{-1} Hz within a simulation time of 10 s. Given that the Ziegler-Nichols method relies on a standard model, the design goals will nearly never be accomplished according to transient response. This method seems to operate best in providing an efficient basis for getting started with controller tuning and does not require expert knowledge or a model of the system before designing the controller. Following Table 1, the Ziegler-Nichols formulation is now applied to obtain the different PID gains depicted in Table 5.

QPSO-LQR PID controller

As can be observed in Fig. 11, the load frequency of the system according to the QPSO-LQR controller achieved better stability in a relatively short amount of time when the load is placed, precisely before 4 s compared to the other controllers that were unable to achieve this amount of stability during this time. Because of the QPSO-LQR optimum control design, the frequency of the load is not significantly altered by the changes that occur in the system parameters, and the load is less than 4 s. The maximum overshoot difference with the LQR controller is also found to be around 0.4521×10^{-1} Hz margin compared to the other approaches. The QPSO-LQR is able to implement a control for dynamic systems with rapidly changing dynamics and fast transients, hence demonstrating the robustness of the controller. The PID gains obtained for the optimal control theory of LQR have been shown in Table 6.

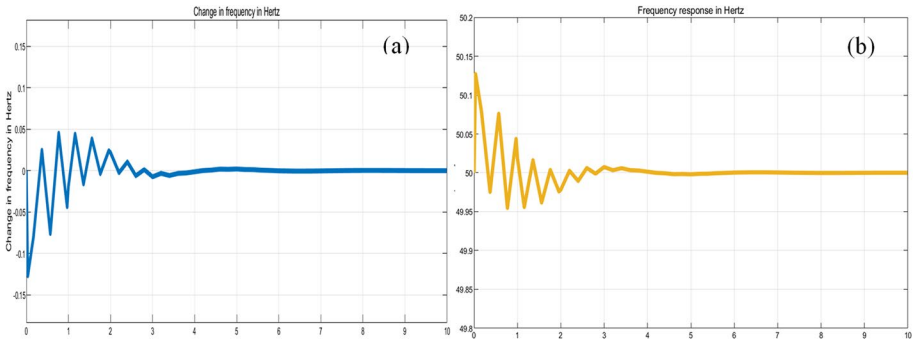

Fig. 11 PID control: LQR-based controller with PSO: 0.2 p.u (50 MW) change in load. **a** Change in frequency in Hz. **b** Measured frequency in Hz

Table 6 PID (classical) control parameter from optimal LQR design from PSO algorithms

Parameter	Value
K_p	79.07627655526
K_i	282.030055079202
K_d	43.7656545844910

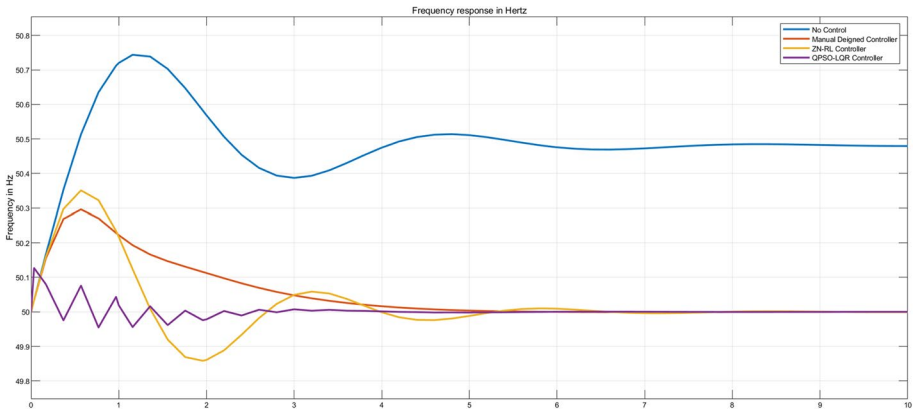

Fig. 12 Combined frequency response of all control action under load change

Validation of proposed QPSO-LQR PID controller

A MATLAB Simulink program has been used to obtain all the above findings for the LFC of an isolated power system. Each of the three distinct cases of an optimal controller design was carried out under the same condition of load change. When observing the performance of a control algorithm, it becomes necessary to compare controller design with other control laws to test its effectiveness in meeting system requirements. It can be seen from Figs. 9, 10, and 11 that the frequency deviation was overall improved when a controller was used compared to the case of no controller action. That is the case in Fig. 9. The combined results of all the controlled case have been presented in Fig. 12.

Table 7 has been used to summarize the results of the transient responses and the controller gains of the different design approaches. In the combined ZN-LR method, a noticeable overshoot of 0.3485 Hz and a steady-state error 0.0007038 Hz after 10 s were found compared to the case of the manual PID controller which had 0.2962-Hz overshoot above the nominal frequency and a steady-state error of 0.0007038 Hz for the

Table 7 Summary of the dynamics of the different controllers and their PID gains

Controller dynamics				
Controller	**No controller**	**Manual**	**ZN-RL**	**QPSO-LQR**
Overshoot (Hz)	0.7437	0.2962	0.3485	0.04521
Steady-state error (Hz)	0.4794	0.0001267	0.0007038	0.00007
Duration of steady-state analysis (s)	10	10	10	10
Controller gains				
PID gains	**Values**			
K_p	-	2.0121	2.244	79.0763
K_i	-	0.9989	2.3194	282.0301
K_d	-	1.0117	0.5428	43.7655

same transient analysis of 10 s. This was however achieved after several trials and efforts of manual tuning. The Ziegler-Nichols method showed lower performance with respect to manual tuning because the method however has been built based on a generic plant model, and design requirements are usually subjective with no standard design rule. The method is also not mathematically rigorous since most of the time a real experiment is usually needed if you do not have the model or simulation of the system; this could be expensive. Also, systems that cannot be driven to instability with proportional gain cannot be designed from this method. On the other hand, the design rule for manual control is non-exhaustive, and the final controller is conclusive in terms of its optimality.

In the case of a QPSO-LQR controller, the frequency has greater stability in a short amount of time following the load change. The maximum overshoot and steady-state error are found to be respectively 0.04521 Hz and 0.00007 Hz which is found to be a significant improvement compared to the manual and ZN-LR designs. The frequency of the load is not significantly altered by the adjustments made to the system parameter with the QPSO-LQR control. The controller produces satisfactory results compared to the manual PID-tuned controller which takes a lot of time to find the best tune and the Ziegler-Nichols method that has been constructed based on a general model that does not consider some of the intrinsic dynamics of the plant.

Conclusions

In this paper, an improved LQR-PID controller has been developed to control the load frequency of a single-area power system. The controller was designed using a QPSO optimization technique. The effectiveness of the suggested control strategy was implemented in the LFC of a single area power system in the presence of external disturbances and parametric uncertainties, as well as load changes. Additionally, the results of damping for frequency deviation profile from the QPSO-based LQR-PID controller were compared with those designed from combined ZN-RL and manual methods. The obtained results confirmed the validity of this strategy. Simulation results show that the proposed QPSO-based LQR-PID controller has a superior control effect of good transient behavior with less overshoot, smaller settling time, and less sensitivity to parameter variations and load disturbances. Moreover, it was discovered that the QPSO-LQR design process was clearer and easier than the conventional controller designs. It should be emphasized that the findings were achieved for all three controllers using different approaches.

The load frequency regulation of two separate power systems linked by a tie line will be considered in the future. Furthermore, before validating its robustness, the suggested technique shall be evaluated with a more sophisticated real-world application such as LFC-integrated electric cars, wind, and solar systems. The power system will be divided into two parts: a microgrid with DGs and the main grid. The intermittent nature of the microgrid power production will be modeled, and an appropriate control law will be developed to control frequency when the load suddenly changes.

Abbreviations

2DOF	Two-degree-of-freedom
BELBIC	Brain emotional learning-based intelligent controller
DG	Distributed generation
DTRS	Desired time response specification
FOPID	Fractional order proportional-integral derivative
ITSE	Integral time square error
LFC	Load frequency control
LQR	Linear quadratic regulator
PI	Proportional integral
PID	Proportional-integral derivative
PI observer	Proportional-integral observer
PSO	Particle swarm optimization
QPSO	Quantum particle swarm optimization
TDC	Transient droop compensator
ZN-RL	Ziegler-Nichols and root locus

Acknowledgements
This investigation did not receive a specific grant from any public, commercial, or nonprofit funding organization.

Authors' contributions
EA contributed to the investigation, data curation, establishing methodology, and formal analysis and was a major contributor to writing the manuscript. WS contributed to the investigation, establishing methodology, supervised the research, validated the resources, and was a major contributor in writing, reviewing, and editing the manuscript. The manuscript was read and approved by both authors.

Funding
The authors received no funding for this work.

Availability of data and materials
All data and materials have been included in the manuscript.

Declarations

Competing interests
The authors declare that they have no competing interests.

Received: 26 June 2023 Accepted: 8 August 2023
Published online: 19 August 2023

References

1. Hassan AS, Othman EA, Bendary FM, Ebrahim MA (2020) Optimal integration of distributed generation resources in active distribution networks for techno-economic benefits. Energy Rep 6:3462–3471. https://doi.org/10.1016/j.egyr.2020.12.004
2. Chauhan J, Surjan BS (2020) Impact of distributed generation in single area load frequency control on system frequency. In: 2020 IEEE International Students' Conference on Electrical, Electronics and Computer Science (SCEECS). IEEE, pp 1–5. https://doi.org/10.1109/SCEECS48394.2020.77
3. Shi Q, Cui H, Li F, Liu Y, Ju W, Sun Y (2017) A hybrid dynamic demand control strategy for power system frequency regulation. CSEE J Power Energy Syst 3(2):176–185. https://doi.org/10.17775/CSEEJPES.2017.0022
4. Homan S, Brown S (2021) The future of frequency response in Great Britain. In: Energy reports. Elsevier Ltd, pp 56–62. https://doi.org/10.1016/j.egyr.2021.02.055
5. Hote YV, Jain S (2018) PID controller design for load frequency control: past, present and future challenges. In: IFAC-PapersOnLine. Elsevier B.V., pp 604–609. https://doi.org/10.1016/j.ifacol.2018.06.162
6. National Instrument (2023) The PID controller & theory explained. https://www.ni.com/de-de/shop/labview/pid-theory-explained.html
7. Xu T, Zhuang Y, Li Y, Zhang E, Kong L (2020) Load-frequency control strategy of power grid with high penetration wind power based on active disturbance rejection control. In: Journal of physics: conference series. Institute of Physics Publishing, pp 1–6. https://doi.org/10.1088/1742-6596/1550/6/062022

8. Hanwate SD, Hote YV (2018) Optimal PID design for load frequency control using QRAWCP approach. In: IFAC-PapersOnLine. Elsevier B.V., pp 651–656. https://doi.org/10.1016/j.ifacol.2018.06.170
9. Hussein AA, Salih SS, Ghasm YG (2017) Implementation of proportional-integral-observer techniques for load frequency control of power system. In: Procedia computer science. Elsevier B.V., pp 754–762. https://doi.org/10.1016/j.procs.2017.05.307
10. Hussain I, Das DC, Latif A, Sinha N, Hussain SMS, Ustun TS (2022) Active power control of autonomous hybrid power system using two degree of freedom PID controller. Energy Rep 8:973–981. https://doi.org/10.1016/j.egyr.2022.05.202
11. Jalali N, Razmi H, Doagou-Mojarrad H (2020) Optimized fuzzy self-tuning PID controller design based on Tribe-DE optimization algorithm and rule weight adjustment method for load frequency control of interconnected multi-area power systems. Appl Soft Comput J 93:106424. https://doi.org/10.1016/j.asoc.2020.106424
12. Oliveira EJ, Honório LM, Anzai AH, Oliveira LW, Costa EB (2015) Optimal transient droop compensator and PID tuning for load frequency control in hydro power systems. Int J Electr Power Energy Syst 68:345–355. https://doi.org/10.1016/j.ijepes.2014.12.071
13. Mohamed A, Abdel-Ghany AG, Bahgat M (2019) Frequency control in a microgrid using decentralized brain emotional learning based intelligent controllers. In: 21stInternational Middle East Power Systems Conference (MEPCON), Tanta University, Egypt. IEEE, pp 265–270. https://doi.org/10.1109/MEPCON47431.2019.9008221
14. Sawarni A, Dhamane K, Kumar D (2019) Decentralized frequency control for an isolated microgrid using nature inspired algorithms. In: IEEE International Conference on Electrical, Computer and Communication Technologies (ICECCT). https://doi.org/10.1109/ICECCT.2019.8869310
15. Saadat H (1999) Power-system-analysis
16. Ellis G (2012) Four types of controllers. In: Control system design guide. Elsevier, pp 97–119. https://doi.org/10.1016/B978-0-12-385920-4.00006-0
17. Kakilli A, Oguz Y, Çalik H (2009) The modelling of electric power systems on the state space and controlling of optimal LQR load frequency. J Electr Electron Eng 9(2):977–982
18. Cheng Z, Li X, Ma J, Teo CS, Tan KK, Lee TH (2019) Data-driven tuning method for LQR based optimal PID controller. In: IECON 2019 - 45th Annual Conference of the IEEE Industrial Electronics Society. IEEE, pp 5186–5191. https://doi.org/10.1109/IECON.2019.8927075
19. Seixas Gomes de Almeida B, Coppo Leite V (2019) Particle swarm optimization: a powerful technique for solving engineering problems. In: Swarm intelligence - recent advances, new perspectives and applications. pp 1–21. https://doi.org/10.5772/intechopen.89633
20. Jordehi AR, Jasni J, Izzri N, Wahab A, Zainal M, Abd A (2013) Particle swarm optimisation applications in FACTS optimisation problem. In: IEEE 7th International Power Engineering and Optimization Conference (PEOCO), pp 193–198. https://doi.org/10.1109/PEOCO.2013.6564541
21. PalupiRini D, MariyamShamsuddin S, SophiyatiYuhaniz S (2011) Particle swarm optimization: technique, system and challenges. Int J Comput Appl 14(1):19–27. https://doi.org/10.5120/1810-2331
22. Kumar S, Sau S, Pal D, Tudu B, Mandal KK, Chakraborty N (2013) Parametric performance evaluation of different types of particle swarm optimization techniques applied in distributed generation system S. In: Proceedings of the International Conference on Frontiers of Intelligent Computing: Theory and Applications (FICTA). pp 349–356. https://doi.org/10.1007/978-3-642-35314-7_40
23. Sun J, Feng B, Xu W (2004) Particle swam optimization with particles having quantum behavior. In: Congress on Evolutionary Computation (IEEE Cat. No.04TH8753). pp 325–331. https://doi.org/10.1109/CEC.2004.1330875
24. Sun J, Xu W, Feng B (2004) A global search strategy of quantum-behaved particle swarm optimization. In: IEEE conference on cybernetics and intelligent systems. pp 111–116. https://doi.org/10.1109/ICCIS.2004.1460396
25. Liu G, Chen W, Chen H, Xie J, Zheng Q (2019) A quantum particle swarm optimization algorithm with teamwork evolutionary strategy. Math Probl Eng 2019:1–13. https://doi.org/10.1155/2019/1805198
26. Patidar H, Mahanti GK, Muralidharan R (2017) Synthesis of non-uniformly spaced linear array of unequal length parallel dipole antennas for impedance matching using QPSO solar photo voltaic cells-extraction of parameters view project synthesis of non-uniformly spaced linear array of unequal length parallel dipole antennas for impedance matching using QPSO. Int J Microw Opt Technol 12(3):172–181. Available:https://www.researchgate.net/publication/317216937.

Publisher's Note